Wearable, Human-Interactive, Health-Monitoring, Wireless Devices Fabricated by Macroscale Printing Techniques

*Wataru Honda, Shingo Harada, Takayuki Arie, Seiji Akita, and Kuniharu Takei**

Wearable human-interactive devices are advanced technologies that will improve the comfort, convenience, and security of humans, and have a wide range of applications from robotics to clinical health monitoring. In this study, a fully printed wearable human-interactive device called a "smart bandage" is proposed as the first proof of concept. The device incorporates touch and temperature sensors to monitor health, a drug-delivery system to improve health, and a wireless coil to detect touch. The sensors, microelectromechanical systems (MEMS) structure, and wireless coil are monolithically integrated onto flexible substrates. A smart bandage is demonstrated on a human arm. These types of wearable human-interactive devices represent a promising platform not only for interactive devices, but also for flexible MEMS technology.

1. Intorduction

Wearable electronics are attractive to realize comfortable, convenient, and secure human life. For example, previous works on flexible devices have focused on sensing and signal processing for artificial electronic eye applications,[1] artificial skin,[2–9] and health-monitoring devices.[10–13] Next-generation wearable electronics for health monitoring will be human-interactive devices that can simultaneously sense signals from the human body (e.g., temperature) and respond to the wearer's needs (e.g., drug delivery or stimulation). However, human-interactive devices have not been explored due to many challenges, including large-scale integration of transistors, sensors, actuators, flexible batteries, and wireless transmitters. To date, transistors on flexible substrates[14–16] with tactile sensors,[2–9] wireless coils,[17,18] or a mechanically flexible battery[19,20] have been reported using organic or inorganic materials. Besides circuits and the battery, wireless signal transmittance and different types of sensors and actuators must be integrated for practical applications of wearable human-interactive devices.

Herein we provide the first proof of concept of a wearable human-interactive device, called a "smart bandage". This device integrates wireless signal transmittance, sensors, and a microelectromechanical systems (MEMS) structure on flexible substrates. After considering costs, a macroscale printing method without standard semiconductor processes (including photolithography) was used for material patterning. The health-monitoring functions include wireless detection of touch and the wearer's skin temperature. Additionally to respond to the wearer's needs, the flexible MEMS structure allows a drug delivery pump (DDP) with a microfluidic channel for drug ejection to be integrated.

W. Honda, S. Harada, Prof. T. Arie, Prof. S. Akita, Prof. K. Takei
Osaka Prefecture University
1–1 Gakuen-cho, Naka-ku, Sakai, Osaka 599–8531, Japan
E-mail: takei@pe.osakafu-u.ac.jp

DOI: 10.1002/adfm.201303874

2. Results and Discussions

This smart bandage integrated a capacitive touch sensor, temperature sensor, and wireless coil for signal transmission to monitor health and a DDP to improve health (**Figure 1**). All components were fabricated on flexible substrates using large-scale lithography-free processes. Briefly, the wireless coil and temperature sensor were printed by screen printing and shadow mask printing on a 15-nm-thick-SiO_2-coated Kapton substrate (250-μm thickness), respectively. Commercially available silver (Ag) ink (Asahi Chem. Res. Lab. Co., Ltd, JAPAN) was used for the coil and to integrate the capacitive touch sensors, which were detected wirelessly. The capacitive touch sensor was patterned on the opposite side of the substrate from where the wireless coil was patterned. To connect the top- and back-surfaces of the substrate, a laser cutting tool (Universal Laser Systems, USA) was used to form via holes through the Kapton substrate. Ag ink was then printed to connect the wireless coil and touch sensor through these vias. The Ag film was printed and baked at 150 °C for 30 min. A touch sensor 3×3 array was also fabricated for the touch panel application on a separate Kapton substrate, as illustrated in Figure 1b. The material for the temperature sensor was synthesized by mixing a conductive poly(3,4-ethylenedioxythiophene):poly(styrenesulfonate) (PEDOT:PSS, 1.3 wt% in water) (Sigma Aldrich, USA) and a carbon nanotube (CNT) paste (SWeNT, USA) with a 10:1 weight ratio. The film after printing was cured at 100 °C for 10 min. DDP with a micro fluidic channel was fabricated using polydimethylsiloxane (PDMS) by a soft lithography as previously reported.[21] Subsequently, the DDP was chemically bonded between Kapton/SiO_2 and PDMS at 100 °C. The PDMS micro pump was strongly bonded onto the Kapton substrate without delamination under bending of a curvature radius 1.5 cm. Finally, the device with a DDP, touch sensor, temperature sensor, and wireless coil was laminated with the touch panel. It should be noted that all processes were carried out

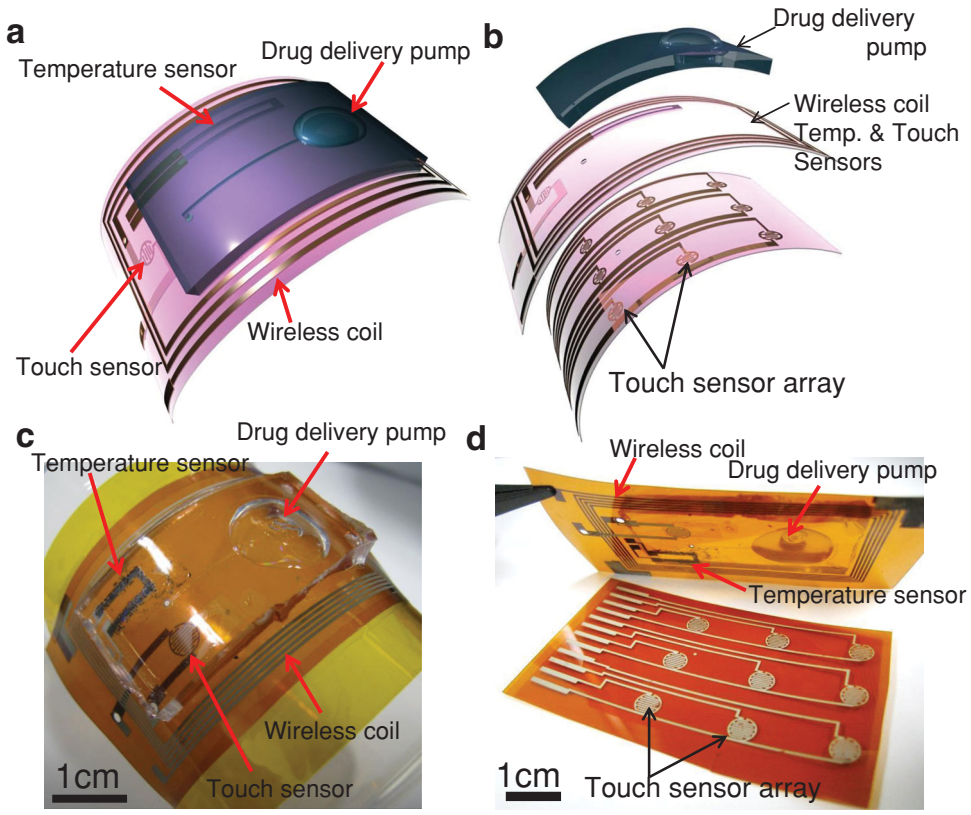

Figure 1. Wearable interactive device ("smart bandage"). Schematics of a smart bandage (a) with and (b) without a capacitive touch panel. Photos of the fabricated smart bandage integrated with touch and temperature sensors, a wireless coil, and a DDP (c) with and (d) without a capacitive touch panel.

under ambient conditions. Figure 1c and d show pictures of the final smart bandage, and confirm that the device can be bent without delamination or cracking.

First, the electrical and mechanical properties of the wireless coil with an integrated touch sensor were characterized using a sender coil (i.e., a smart bandage) and a receiver coil (**Figure 2**a). The capacitive touch sensor was connected in series to the sender coil (Figure 2a inset). The sheet resistance of the printed Ag electrode (~17-μm thick) was 63 ± 4.6 mΩ/square. Both the sender and receiver coils desinged 49 mm × 28 mm with a 400-μm electrode width and 300-μm gap between the electrodes. Five turns of the coil resulted in a total resistance and inductance of R~101 Ω and L~1.03 μH, respectively.

To understand the resonant frequency of the coils, the S-parameter of the transmitting signal through the receiver coil (i.e., S_{21}) was measured. Figure 2b shows that the resonant frequency of S_{21} was around 53.6 MHz with ~0.5-mm distance between the sender and receiver coils. Touching the touch sensor clearly altered the resonant frequency from 53.6 MHz to 53.4 MHz. Additionally, the peak amplitude of the S_{21} signal was changed. These results suggest that device can detect an object or human touch wirelessly via the coils.

The output voltage as a function of coil distance without touching was measured by applying a transmitted alternating current (AC) signal of 42 MHz and 2 V. It should be noted that the AC frequency varied slightly from the result in Figure 2b because the measurement setups differed, altering the parasitic capacitance and conductance of the electrical wire. The 42 MHz frequency showed the largest transmitted signal peak through the receiver coil for this setup. The amplitude of the received signal linearly decreased as a function of coil distance from 0.5 mm to 30 mm at a rate of ~1.2 mV/mm (~3.3%/mm) (Figure 2c). This behavior agrees well with other reports on wireless transmittance.[17] For practical measurements, the output signals were also characterized. There is a 1.6-mV amplitude difference and a 44° phase shift with and without touching the touch sensor (Figure 2d), confirming that the device can successfully detect a touch wirelessly.

To realize highly reliable wearable devices, the mechanical flexibility of the screen-printed Ag electrode on Kapton is an important factor. Figure 2e shows the normalized change in resistance of the Ag electrode, $\Delta R = (R-R_0)/R_0$, by bending the substrate with a curvature radius up to 0.5 mm, where R and R_0 are the resistance at the bent and relaxed states, respectively. The difference in output resistance was negligible for a bend with >0.5-mm radius. This stability is attributed to the high-density porous structure of the Ag film, which is formed unintentionally as printed (Figure 2e inset) and creates a mechanical flexibility similar to a sponge.

Next, the printed resistive temperature sensor using PEDOT:PSS and CNT ink was characterized. The temperature sensor was patterned by shadow mask printing using a PDMS mold (**Figure 3**a). The change in resistance was measured as a function of temperature. Figure 3b shows the normalized

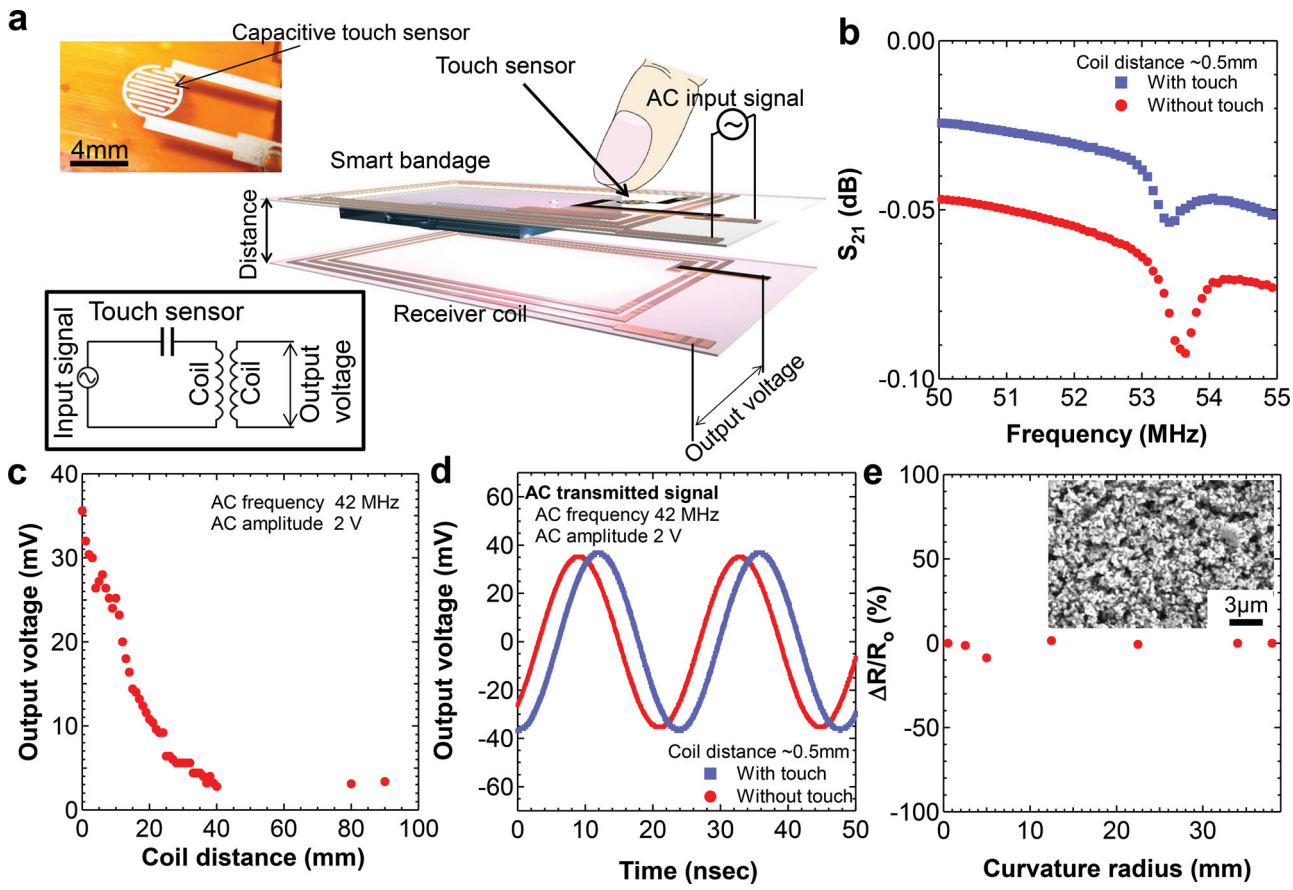

Figure 2. Wireless coils integrated with a capacitive touch sensor. (a) Schematic of the measurement setup. Insets show a photo of a capacitive touch sensor (top) and a circuit diagram of a wireless touch sensor (bottom). (b) S_{21} parameter transmitted from the smart bandage to the receiver coil with a distance ~0.5 mm with and without touching the touch sensor. (c) Output voltage as a function of coil distance. (d) Output AC signal with and without touching. (e) Normalized resistance change in the Ag electrode by bending the substrate up to 0.5-mm radius of curvature. Inset is a scanning electron microscopy (SEM) image of the screen-printed Ag electrode film.

resistance change, $\Delta R/R_0$, by changing the temperature from room temperature (R.T. ~ 22 °C) to 48 °C and vice versa, where $\Delta R = R–R_0$ and R and R_0 are resistance at measured temperature and R.T., respectively. The temperature ranged between R.T. and ~50 °C because this device application is intended as a human interface, which does not require measurements above 50 °C. The sensitivity was ~0.61%/°C, and Figure 3b indicates a negligible hysteresis upon increasing and decreasing the temperature. This sensitivity is slightly better than that of a Pt thermal sensor (~0.53%/°C) fabricated on a flexible substrate[13] although the sensor in this study was fabricated by a large-scale printing method.

The mechanism of the resistance change is most likely 1) a standard temperature–resistance dependence of the materials based on the temperature coefficient of resistance and 2) electron hopping at the interface between PEDOT:PSS and CNTs. In fact, when a PEDOT:PSS or CNT paste was individually used for the temperature sensor, the sensitivity was ~0.4%/°C or ~0.18%/°C, respectively, which is lower than that of a PEDOT:PSS/CNT mixed temperature sensor. These results confirm that PEDOT:PSS and CNT have insufficient temperature coefficients necessary to achieve a sensitivity of 0.61%/°C, and high sensitivity of the mixed sensor is most likely due to the interface between these materials. However, to fully understand the detailed mechanism, more characterization is required. A repeated cycle test at ambient pressure between R.T. (varied between 22 °C and 24 °C) and ~50 °C (49–53 °C) confirmed that the temperature sensor was electrically stable. In addition, the mechanical flexibility, which was measured similar to that shown in Figure 2e, showed that the temperature sensor was mechanically flexible without a resistance change up to ~3.6 mm radius.

The proposed smart bandage included a drug-delivery function by integrating a DDP fabricated by MEMS technology. The drug ejection rate and mechanical flexibility as functions of applied pressure onto the pump and bending radius were analyzed because this is the first demonstration where a MEMS DDP device are integrated on flexible substrates. The semisphere drug reservoir with a volume of ~0.2 mL worked as a pump. **Figure 4**a shows the dimensions of the microfluidic channel. By applying pressure onto the DDP, the dyed water, which imitated a drug, was ejected from the bottom surface of the Kapton substrate through a microchannel (Figure 4b).

The finite element method (FEM: COMSOL Multiphysics 4.2a) was used to simulate the deformation of the PDMS DDP upon applying pressure onto the DDP structure. Applying a

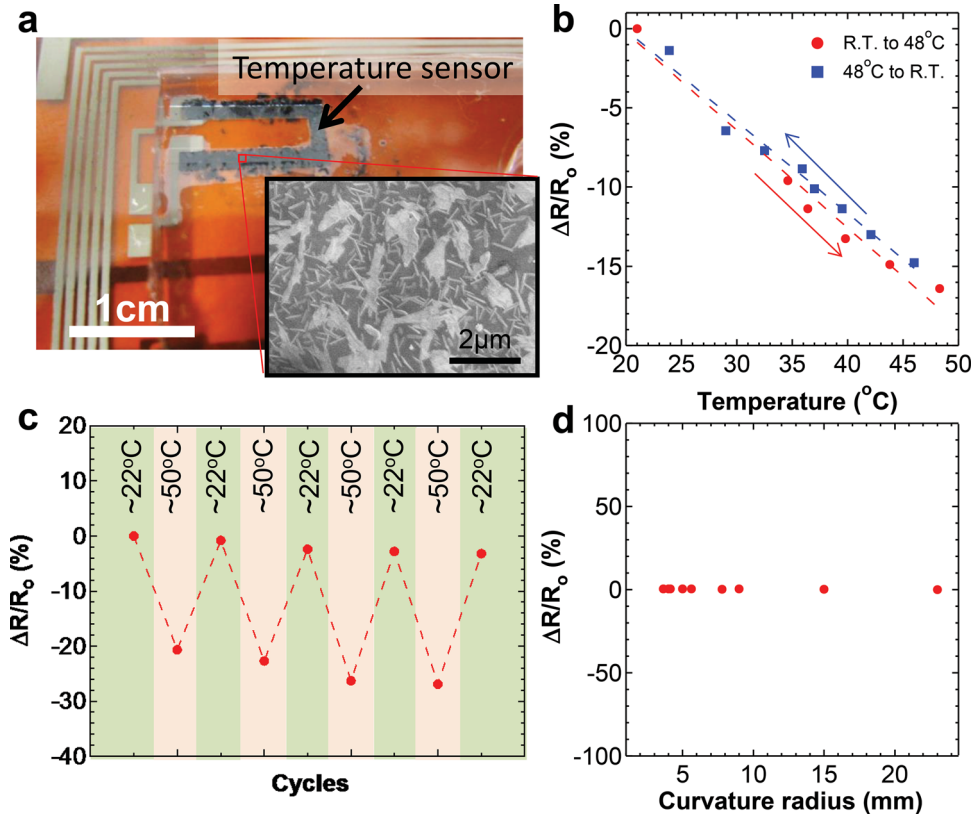

Figure 3. Temperature sensor. (a) Photo of a temperature sensor. Inset is a SEM image of mixed film of PEDOT:PSS and CNT ink. Crystallization of PEDOT:PSS and CNT bundles are observed on the surface of the film. (b) Normalized resistance change as a function of temperature. (c) Cycle test of the temperature sensor as the temperature changes from R.T. (~22–24 °C) to ~49–53 °C. (d) Mechanical flexibility normalized resistance change of the temperature sensor upon bending the device up to a 3.6-mm radius.

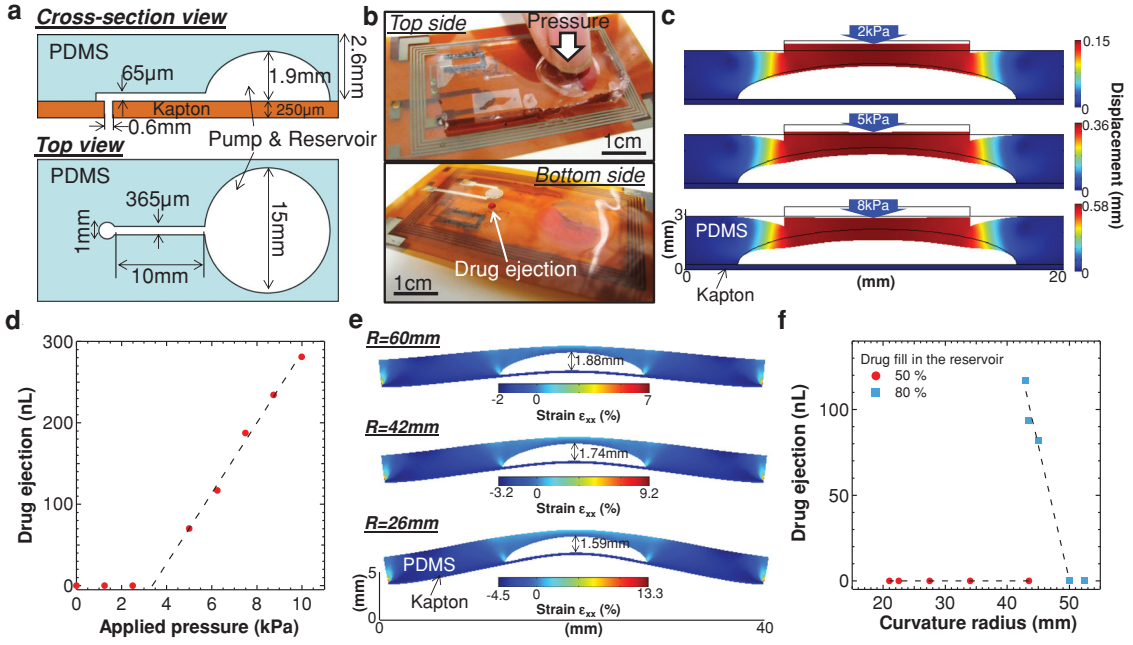

Figure 4. Drug delivery pump. (a) Schematic of PDMS-based pump/reservoir and microfluidic channel. (b) Photos of dyed water ejection by applying the pressure onto the pump. (c) FEM results by applying the pressure from 2 kPa to 8 kPa. Color difference indicates displacement of the PDMS pump structure. (d) Experimental drug (dyed water) ejection as a function of pressure. (e) FEM results to observe the height of pump/reservoir with different bending radii. Color difference indicates the strain distribution due to bending. (f) Ejection as a function of the bending radius with the reservoir 50% and 80% full.

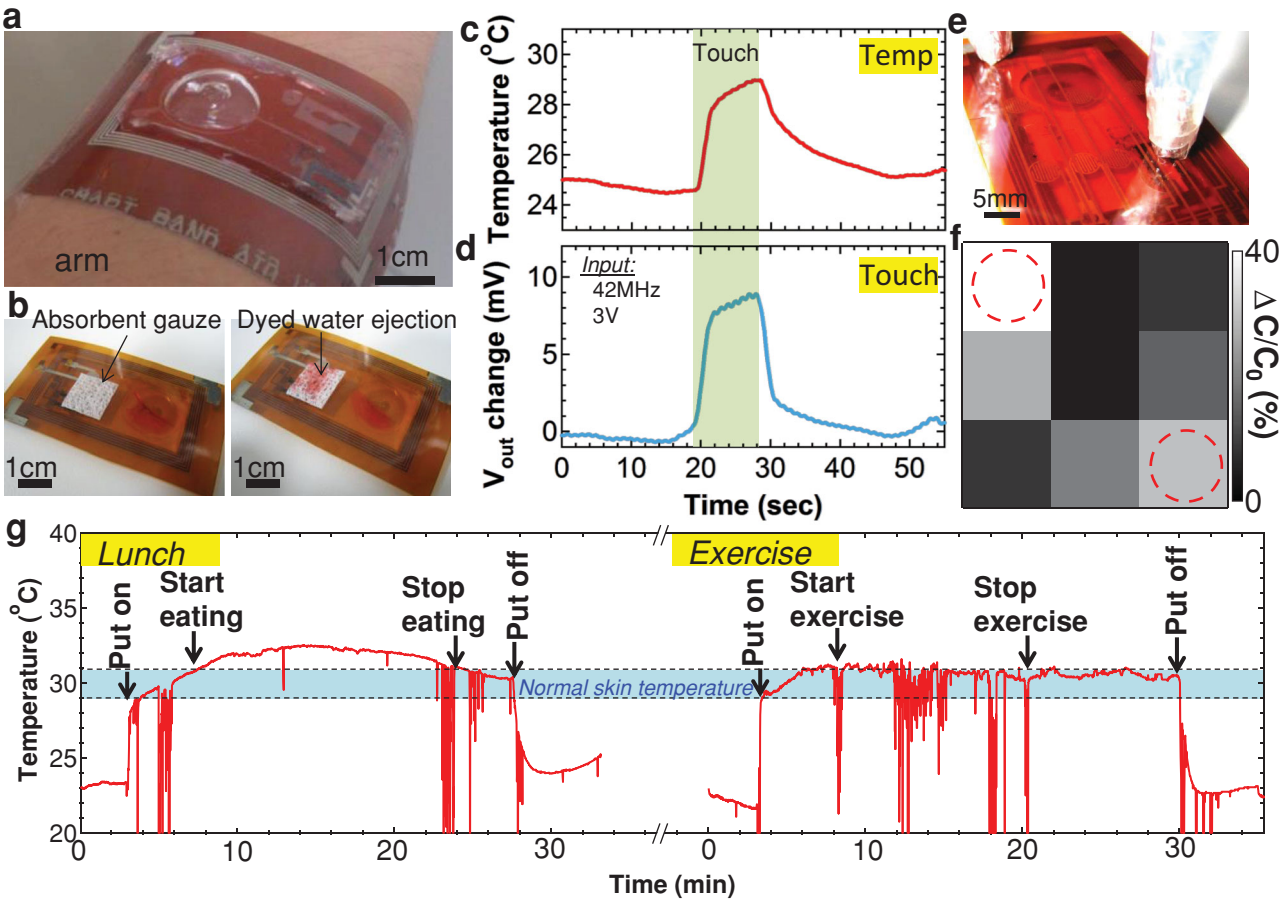

Figure 5. Smart bandage demonstration. (a) Final device structure on a human arm. (b) Before and after water ejection from DDP. (c,d) Simultaneous temperature and wireless touch detection. (e) (f) Capacitive touch sensor 3×3 array for a touch panel application and the two-dimensional touch distribution based on the normalized capacitance change. Circles with dashed lines indicate the touch regions. (g) Real-time temperature measurement of a skin surface (adult male) during lunch and exercise. Artificial noise is most generated due to a bad electrical contact in the measurement setup.

pressure of ~2 kPa deformed PDMS only slightly (Figure 4c), but applying a pressure >5 kPa clearly decreased in the height of the drug reservoir/pump, resulting in a decrease in the reservoir volume. The ejection rate was experimentally confirmed (Figure 4d). The threshold pressure to eject a drug and the ejection rate were ~3.3 kPa and ~35 nL/kPa, respectively. The threshold pressure is within the range of a gentle human touch, indicating that this DDP can be operated by anybody, including a child. To control the amount of drug into human body as a practical use, a pre-chamber with one-way fluidic valve, which controls the volume of drug from the DDP, should be integrated in the future.

To further elucidate the flexible MEMS structure of DDP, the mechanical flexibility of a reservoir filled with water was studied using FEM analysis and experiments. A bending radius of ~60 mm did not significantly alter the reservoir height (Figure 4e). However, decreasing the bending radius decreased the height due to bending a flexible substrate and the PDMS structure. The threshold radius to eject a drug by bending the substrate depended on the drug volume in the reservoir (Figure 4f). When the reservoir volume was 80% full (~160 μL), the threshold was around 50 mm, but was <22 mm when the reservoir was 50% full (~100 μL) because the decreased reservoir height corresponded to the reservoir volume upon bending the substrates. These results suggest that for safety the drug should be filled after placing the smart bandage on the skin or the drug volume should be controlled based on the curvative radius where the smart bandage is placed.

As a proof-of-concept of a smart bandage, all components (wireless coil, DDP, and touch and temperature sensors) were monolithically integrated on a flexible substrate via lithography-free printing processes. **Figure 5**a shows the final device structure. For the bandage, an absorbent gauze was placed on the drug outlet, and dyed water could be ejected from the DDP (Figure 5b). When drug is needed to deliver into human body, a painless flexible microneedle should be integrated using MEMS techniques[22] as an example for the future. The temperature and touch detections were simultaneously initiated upon touching a sensor with a finger. Touch detection was wirelessly recorded from the smart bandage to the receiver coil as described in Figure 2a. The transmitted signal was 42 MHz and 3 V. Figures 5c and d show the output signals from both sensors; the longest response time based on the temperature sensor was ~18 s, which is high enough for a health-monitoring system. However, the temperature sensor response could be improved by considering the device geometry.

Additional applications of the smart bandage were also considered. A flexible touch panel, a capacitive touch sensor 3×3 array was fabricated and laminated under the smart bandage. By placing two objects on the substrate, the two-dimensional tactile distribution could be measured (Figure 5e,f).

Finally, real-time temperature measurements from human skin were examined by placing a smart bandage connected to a compact voltage recorder onto an adult male's arm. The sampling frequency was 1 Hz, and a 9 V battery was used for the measurement. The skin surface temperature was successfully monitored (Figure 5g). The experiment was conducted in a room at ~23 °C. A normal skin temperature is ~29–31 °C, but the subject's skin temperature during lunch (eating spicy soup) increased to ~32.5 °C, most likely due to the release of heat to control body temperature. Interestingly, a smaller increase in skin temperature was observed during exercise than that during lunch. This is probably because the exercise time of ~12 min is not long enough to observe the increase of skin temperature based on the heat release from the human body at relatively comfortable air ambient (~23 °C). However lunch with spicy soup caused strong perspiration from human body through the skin compared to the short-time exercise. By integrating the device on a flexible substrate with a simple measurement system, real-time measurements during human activity and small changes in skin temperature were successfully detected.

3. Conclusion

Here, we proposed and demonstrated a smart bandage with a drug delivery function as an application of a wearable human-interactive health-monitoring wireless device. Although photolithography-free cost-effective printing techniques were used, the device was successfully integrated with a similar or better performance compared to other sensors fabricated by conventional semiconductor process. In addition, the flexible MEMS device concept should realize a new function for flexible electronics. Although this study did not integrate transistors, previous studies[14,16] indicate that transistors should be readily incorporated in the future. Consequently, this human-interactive "smart bandage" concept should play an important role for future wearable electronics and contribute to medical technology.

Acknowledgements

This work was partially supported by the Foundation Advanced Technology Institute and JSPS KAKENHI Grant (#25889048).

Received: November 15, 2013
Revised: December 19, 2013
Published online: February 28, 2014

[1] Y. M. Song, Y. Xie, V. Malyarchuk, J. Xiao, I. Jung, K.-J. Choi, Z. Liu, H. Park, C. Lu, R.-H. Kim, R. Li, K. B. Crozier, Y. Huang, J. A. Rogers, *Nature* **2013**, *497*, 95.
[2] K. Takei, T. Takahashi, J. C. Ho, H. Ko, A. G. Gillies, P. W. Leu, R. S. Fearing, A. Javey, *Nature Mater.* **2010**, *9*, 821.
[3] C. Wang, D. Hwang, Z. Yu, K. Takei, J. Park, T. Chen, B. Ma, A. Javey, *Nature Mater.* **2013**, *12*, 899.
[4] S. C. B. Mannsfeld, B. C.-K. Tee, R. M. Stoltenberg, C. V. H.-H. Chen, S. Barman, B. V. O. Muir, A. N. Sokolov, C. Reese, Z. Bao, *Nature Mater.* **2010**, *9*, 859.
[5] M. L. Hammock, A. Chortos, B. C.-K. Tee, J. B.-H. Tok, Z. Bao, *Adv. Mater.* **2013**, *25*, 5997.
[6] R. C. Webb, A. P. Bonifas, A. Behnaz, Y. Zhang, K. J. Yu, H. Cheng, M. Shi, Z. Bian, Z. Liu, Y.-S. Kim, W.-H. Yeo, J. S. Park, J. Song, Y. Li, Y. Huang, A. M. Gorbach, J. A. Rogers, *Nature Mater.* **2013**, *12*, 938.
[7] M. Kaltenbrunner, T. Sekitani, J. Reeder, T. Yokota, K. Kuribara, T. Tokuhara, M. Drack, R. Schwodiauer, I. Graz, S. Bauer-Gogonea, S. Bauer, T. Someya, *Nature* **2013**, *499*, 458.
[8] T. Someya, T. Sekitani, S. Iba, Y. Kato, H. Kawaguchi, T. Sakurai, *Proc. Natl. Acad. Sci. USA* **2004**, *101*, 9966.
[9] W. Wu, X. Wen, Z. L. Wang, *Science* **2013**, *340*, 952.
[10] G. Schwartz, B. C.-K. Tee, J. Mei, A. L. Appleton, D. H. Kim, H. Wang, Z. Bao, *Nat. Commun.* **2013**, DOI: 10.1038/ncomms2832.
[11] C. Pang, G.-Y. Lee, T. Kim, S. M. Kim, H. N. Kim, S.-H. Ahn, K.-Y. Suh, *Nature Mater.* **2012**, *11*, 795.
[12] T. Yamada, Y. Hayamizu, Y. Yamamoto, Y. Yomogida, A. Izadi-Najafabadi, D. N. Futaba, K. Hata, *Nature Nanotechnol.* **2011**, *6*, 296.
[13] D.-H. Kim, N. Lu, R. Ghaffari, Y.-S. Kim, S. P. Lee, L. Xu, J. Wu, R.-H. Kim, J. Song, Z. Liu, J. Viventi, B. de Graff, B. Elolampi, M. Mansour, M. J. Slepian, S. Hwang, J. D. Moss, S.-M. Won, Y. Huang, B. Litt, J. A. Rogers, *Nature Mater.* **2011**, *10*, 316.
[14] M. Jung, J. Kim, J. Noh, N. Lim, C. Lim, G. Lee, J. Kim, H. Kang, K. Jung, A. D. Leonard, J. M. Tour, G. Cho, *IEEE Trans. Electron Dev.* **2010**, *57*, 571.
[15] D.-M. Sun, M. Y. Timmermans, A. Kaskela, A. G. Nasibulin, S. Kishimoto, T. Mizutani, E. I. Kauppinen, Y. Ohno, *Nat. Commun.* **2013**, *4*, 2302.
[16] P. H. Lau, K. Takei, C. Wang, Y. Ju, J. Kim, Z. Yu, T. Takahashi, G. Cho, A. Javey, *Nano Lett.* **2013**, *13*, 3864.
[17] T. Sekitani, M. Takamiya, Y. Noguchi, S. Nakano, Y. Kato, T. Sakurai, T. Someya, *Nature Mater.* **2007**, *6*, 413.
[18] S.-W. Hwang, H. Tao, D.-H. Kim, H. Cheng, J.-K. Song, E. Rill, M. A. Brenckle, B. Panilaitis, S. M. Won, Y.-S. Kim, Y. M. Song, K. J. Yu, A. Ameen, R. Li, Y. Su, M. Yang, D. L. Kaplan, M. R. Zakin, M. J. Slepian, Y. Huang, F. G. Omenetto, J. A. Rogers, *Science* **2012**, *337*, 1640.
[19] Y. Yang, S. Jeong, L. Hu, H. Wu, S. W. Lee, Y. Cui, *Proc. Natl. Acad. Sci. USA* **2011**, *108*, 13013.
[20] A. M. Gaikwad, G. L. Whiting, D. A. Steingart, A. C. Arias, *Adv. Mater.* **2011**, *23*, 3251.
[21] K. Iwai, R. D. Sochol, L. Lin, *Proc. MEMS 2011 conf.* **2011**, 1131.
[22] B. Stoeber, D. Liepmann, *J. Microelectromech. Syst.* **2005**, *14*, 472.